Applied Catalysis B: Environmental 89 (2009) 149–159

Contents lists available at ScienceDirect

Applied Catalysis B: Environmental

journal homepage: www.elsevier.com/locate/apcatb

The effect of CeO_2 on the surface and catalytic properties of Pt/CeO_2–ZrO_2 catalysts for methane dry reforming

S. Damyanova [a,*], B. Pawelec [b], K. Arishtirova [a], M.V. Martinez Huerta [b], J.L.G. Fierro [b]

[a] Institute of Catalysis, Bulgarian Academy of Sciences, Acad. G. Bonchev str. block 11, 1113 Sofia, Bulgaria
[b] Instituto de Catalisis y Petroleoquimica, CSIC, Cantoblanco, 28049 Madrid, Spain

ARTICLE INFO

Article history:
Received 29 September 2008
Received in revised form 25 November 2008
Accepted 30 November 2008
Available online 6 December 2008

Keywords:
Dry reforming
Methane
Pt catalysts
Zirconia
Ceria–zirconia substrates

ABSTRACT

The CO_2 reforming of CH_4 over Pt catalysts supported on nanocrystalline mesoporous ZrO_2 and CeO_2–ZrO_2 carriers was investigated at atmospheric pressure. The effect of CeO_2 content (1–12 wt%) on the surface and catalytic properties of the catalysts was studied. It was found that the pre-treatment temperature and the concentration of CeO_2 influence on the morphology of Pt particles. The calcination temperature as high as 1073 K leads to sintering of Pt particles deposited over zirconia- and CeO_2-loaded zirconia substrates. Temperature-programmed reduction (TPR) results showed good reductive properties for Pt/CeO_2–ZrO_2 catalysts due to both, the high surface shell reduction of zirconia and the synergetic effect between Pt and CeO_2. X-ray photoelectron spectroscopy (XPS) of reduced catalysts revealed the presence of different Pt oxidation state depending on the catalyst composition. Stabilization of partially oxidized platinum species by ceria was detected for the reduced Pt/CeO_2–ZrO_2 samples. An activation period was required for the stabilization of the activity of Pt/CeO_2–ZrO_2 catalysts. The high stability of Pt/CeO_2–ZrO_2 catalysts was related to the close contact between Pt and CeO_2.

1. Introduction

Methane, the main component of the natural gas is widely used as a feedstock for petrochemical manufacturing. Indirect utilization of natural gas via syngas is the main route to convert methane to liquid fuels, ammonia, methanol, etc. Industrially, syngas is mainly produced by steam reforming of methane. However, the H_2/CO ratio of 3:1 by this method is higher than what is needed for the downstream synthesis process. CO_2 reforming of methane is an alternative to steam reforming, which gives a low H_2/CO ratio ($\approx$1) [1–3]. It follows that by suitable combination of steam and CO_2 reforming it should be possible to achieve the most favourable H_2/CO ratio for required applications.

Currently the development of CO_2 reforming is hindered by the absence of suitable catalysts that provide high activity and selectivity. Other advantages of CO_2 reforming are that CO_2 is consumed, rather than being produced and, it has potential in the co-utilization of coal bed methane. It can be used for the chemical energy storage [4], due to the high endothermicity of the reaction. In view of these potential advantages, it is likely that CO_2 reforming will become increasingly important in the future.

Many investigations on CO_2 reforming of methane over supported metal catalysts have been reported. Industrially, nickel-based catalysts have been used for reforming reactions as they are relatively cheap and possess high activity [2,3,5,6]. However, due to the high-temperature reaction of the reforming process, the nickel catalysts deactivate quickly due to sintering of the active metal phase and coke deposition. Studies have shown that supported noble metals have been used successfully in the reaction of CO_2 reforming of methane, but their activity and stability depends strongly on the kind of the carrier [2,7–10].

It is well known, that the structure and surface properties of the support exert an important influence on the catalytic activity of supported catalyst. Therefore, the search of new catalysts supported on suitable carrier is still a research priority. The most commonly used support for CO_2 reforming is Al_2O_3. However, other oxides recently explored such as ceria and zirconia have attracted attention as carriers or catalysts for important industrial or environmentally friendly reactions [11–17]. It is known that these oxides can impart metal–support interactions to enhance catalytic performances, due to the oxygen-storage/transport characteristics of the support or to the generation of active centres at the interface between metal and support. In addition, ceria and ceria-based substrates may improve the catalytic performances by increasing metal dispersion [18]. Thus, to take the advantage of the metal–support synergistic effect in the reaction of CO_2 reforming of methane appears to be appropriate to develop a catalyst that is resistant to carbon deposition and exhibits stable activity with time on stream.

* Corresponding author. Tel.: +359 29792588; fax: +359 29712967.
E-mail address: sonia.damyanova@yahoo.com (S. Damyanova).

0926-3373/$ – see front matter © 2009 Elsevier B.V. All rights reserved.
doi:10.1016/j.apcatb.2008.11.035

However, the major problem of CeO_2 is to lose its oxygen storage capacity due to a decrease of its surface area under high thermal treatment and reductive atmosphere. Deposition of ceria on a support with a high surface area leads to obtain carriers with a high surface area and good redox properties [19]. On other hand, the use of support with low concentration of Lewis acid sites and/or presence of basic sites results in enhancement of catalyst activity, lower coke deposition and therefore more stable catalysts. Among these supports, ZrO_2 can be successfully used as a catalyst support. In the literature there are few reports about the use of ZrO_2 with a high surface area for catalytic applications.

The present work is a prolongation of our studies over supported Pt catalysts for dry methane reforming. We attempted to deposit ceria on mesoporous nanocrystalline zirconia and to obtain CeO_2–ZrO_2 supports with high surface areas [19]. After that Pt catalysts supported on pure ZrO_2 and CeO_2–ZrO_2 oxides with different CeO_2 content have been prepared. The aim of the present work is to evaluate the role of the support in Pt/CeO_2–ZrO_2 catalysts on their surface and catalytic properties in the reaction of CH_4 reforming with CO_2. X-ray diffraction (XRD), Raman and X-ray photoelectron spectroscopy (XPS), temperature-programmed reduction (TPR) and thermogravimetric analysis (TGA) have been used for characterization of the samples.

2. Experimental

2.1. Sample preparation

ZrO_2 support, kindly offered from Eurosupport (The Netherlands) was calcined at 823 K for 4 h. The CeO_2–ZrO_2 supports were obtained by impregnation of ZrO_2 with an aqueous solution of diammonium hexanitrato cerate $(NH_4)_2[Ce(NO_3)_6]$ (99.99% pure from Degussa) at room temperature [19]. The obtained solids were dried in air at 383 K for 12 h and were calcined at 823 K for 4 h. The theoretical amount of CeO_2 was in the range of 1–12 wt%. For comparison a bulk CeO_2 was obtained by calcination of $(NH_4)_2[Ce(NO_3)_6]$ at 923 for 4 h. Pt catalysts supported on ZrO_2, CeO_2 and CeO_2–ZrO_2 oxides were prepared by wet impregnation of the carriers with a solution of $H_2PtCl_6{\cdot}6H_2O$ in ethanol at room temperature. Appropriate amount of the carrier was added to the solution of Pt salt and the mixture was stirred in a rotavapor during 2 h at room temperature. After that the ethanol was evaporated at 333 K. The solids were dried and calcined at 383 and 773 K for 8 and 2 h, respectively. All the catalysts had the same Pt loading of about 1 wt%. The samples were denoted as Pt/xCeO_2–ZrO_2, where x is the theoretical CeO_2 content.

2.2. Experimental techniques

Inductively Coupled Plasma Atomic Emission Spectroscopy (ICP-AES) using a PerkinElmer Optima 3300DV instrument determined the chemical analysis of the calcined catalysts. The solid samples were treated with a mixture of HF, HCl and HNO_3 at 363 K and homogenized in a microwave oven. The textural properties of the calcined catalysts were determined from the nitrogen adsorption–desorption isotherms recorded at 77 K with a Micromeritics TriStar 3000 apparatus. The samples were previously degassed at 423 K for 24 h under a vacuum (10^{-4} mbar) to ensure a clean dry surface, free of any loosely bound adsorbed species. The specific areas of the samples were determined according standard BET procedure using nitrogen adsorption data taken in the relative equilibrium pressure interval of $0.03 < P/P^0 < 0.3$.

XRD measurements of the calcined catalysts were performed on a computerized Seifert 3000XRD diffractometer using Cu Kα (λ = 1.538 Å) radiation and a PW 2200 Bragg-Brentano $\theta/2\theta$ goniometer equipped with a bent graphite monochromator and an automatic slit. The XRD diffraction patterns were taken in the 2θ range of 5–80° at a scan speed of 0.04°/s. Phase identification was carried out by comparison with the JCPDF data base cards. Particle size of CeO_2 and ZrO_2 crystallites were determined by means of the Scherrer equation [20] using the most intensive reflections. The Raman spectra were run with a Renishaw Micro-Raman System 1000 equipped with a cooled CCD detector and a holographic Notch filter that removes the elastic scattering. The samples were excited with the 514 nm Ar line in an *in situ* cell (Linkam, TS-1500), which allows temperature treatments up to 1773 K under flowing gases. The samples were in powder form to prevent diffusion problems and ensure that all catalyst in the cell is exposed to the flowing gases. The spectral resolution is 3 cm^{-1}, and the spectra acquisition consisted of 20 accumulations of 30 s for each sample. The samples calcined at 1073 K were pre-treated in air at 773 K for 30 min.

X-ray photoelectron spectra of freshly H_2-reduced (*in situ* at 773 K) catalysts and spent ones were recorded on a VG Escalab 200R electron spectrometer equipped with a hemispherical electron analyzer, using a Mg Kα ($h\nu$ = 1253.6 eV, 1 eV = 1.603×10^{-19} J) X-ray source. After degassing at 10^{-6} mbar, the samples were transferred to the ion-pumped analysis chamber, in which residual pressure was kept below 4×10^{-9} mbar during data acquisition. The binding energies (BEs) of Zr 3d, Ce 3d and Pt $4d_{5/2}$ core-levels were measured with respect the binding energy of the C 1s peak of adventitious carbon at 284.9 eV taken as an internal standard. The accuracy of the BE values was ±0.1 eV. The invariance of the peak shapes and widths at the beginning and at the end of the analyses indicated constant charge along measurements. The peaks were fitted by a non-linear least square fitting routine using a properly weighted sum of Lorentzian and Gaussian component curves after background subtraction according to Shirley [21] and Sherwood [22]. Surface atomic concentration was evaluated from peak areas using appropriate sensitivity factors built in the VG instrument software.

Temperature-programmed reduction profiles of the calcined samples were obtained on a semiautomatic Micromeritics TPD/TPR 2900 apparatus interfaced with a computer. TPR profiles were recorded on the previously degassed (He, 473 K, 0.5 h) sample (0.05 g) by passing a 10 wt% H_2/Ar gas mixture (60 ml/min) through the sample heated at a constant rate of 15 K min^{-1} from room temperature to 1273 K. A cold trap was placed before the thermo-conductivity detector (TCD) to remove water from the exit stream. In order to evaluate the formation of carbon we carried out thermogravimetric analysis experiments of the spent catalysts with a TGA/SDTA 851^e Mettler Toledo apparatus. Temperature-programmed oxidation (TPO) tests of the spent catalysts have been carried out in a 20% O_2/N_2 mixture by raising the temperature from room temperature to 1073 K at a rate of 10 K/min.

2.3. Catalytic reaction

The catalytic experiments in the reaction of CH_4 reforming with CO_2 were performed at atmospheric pressure. The catalyst sample with particle diameter in the range from 0.2 to 0.25 mm was diluted with quartz tips (0.2–0.3 mm) and was packed in a fixed-bed continuous flow reactor (quartz tube with an inner diameter of 6 mm and a length of 300 mm). The amount of the catalyst used during the catalytic runs was 0.05 g. It was worked at low conversions values in order to achieve maximal differences in the activity of the studied catalyst samples with similar properties. Before each catalytic test, the catalyst was reduced *in situ* by heating the catalyst in a stream of 50 ml/min 10% H_2/N_2, from room temperature to 773 K at a rate of 10 °C/min and maintaining this temperature for 1 h. After reduction, the catalyst was purged with flowing nitrogen (60 ml/min) for 40 min to remove physically

adsorbed hydrogen from the surface. The activity test was performed at 823 K with a reactant gas mixture of CH_4 (20%) and CO_2 (20%) diluted with N_2. The total flow rate was always kept at 100 ml/min. The reaction products were analyzed be means of a gas chromatograph (Varian 3700) equipped with a 3 m active carbon column (Carlo Erba) and a TCD. The catalytic properties have been evaluated in terms of CH_4 and CO_2 conversions; H_2 and CO yields as follows:

$$CH_4\ \text{conversion}\ (\%) = \frac{(CH_4)_{in} - CH_4)_{out}}{(CH_4)_{in}} 100 \quad (1)$$

$$CO_2\ \text{conversion}\ (\%) = \frac{(CO_2)_{in} - (CO_2)_{out}}{(CO_2)_{in}} 100 \quad (2)$$

$$H_2\ \text{yield}\ (\%) = \frac{(H_2)_{out}}{(CH_4)_{in}} \frac{100}{2} \quad (3)$$

$$CO\ \text{yield}\ (\%) = \frac{(CO)_{out}}{(CH_4)_{in}} + (CO_2)_{in} \quad (4)$$

3. Results

3.1. Textural characteristics

The shape of the N_2 adsorption–desorption isotherms of Pt/ZrO_2 and Pt/CeO_2–ZrO_2 catalysts is similar to that of ZrO_2 (the figure is not shown). According to the IUPAC classification the N_2 isotherms of all samples are of type II/IV, characterizing macro- and mesoporous solids, respectively [23]. The isotherms of the samples have hysteresis loops that according to IUPAC are near to H1/H2 type, which is characteristic for mesoporous/macroporous materials [23].

BET specific surface areas (S_{BET}) and pore volumes (V_p) of supported Pt catalysts are listed in Table 1. For comparison, the surface areas of CeO_2–ZrO_2 carriers [19] are also presented in Table 1. In our previous study [19] the stabilization effect of CeO_2 up to 6 wt% on the textural properties of modified ZrO_2 with CeO_2 was shown. The same trend in the change of S_{BET} with increasing the CeO_2 content is observed for Pt/CeO_2–ZrO_2 samples. The sample with the highest CeO_2 content (12 wt%) has the lowest surface area value that would be attributed to the blockage of the pores of ZrO_2 with cerium oxide particles. Stabilization of the ZrO_2 phase by addition of small quantities of another oxides, such as Y_2O_3 and CeO_2, has been previously reported [24,25]. In addition, the stabilization effect of CeO_2 at low concentrations (1–3 wt%) on the textural and thermal properties of Al_2O_3 has been also observed [8].

The treatment of the samples at high temperature of 1073 K leads to a decrease of the surface areas and pore volumes of Pt/CeO_2–ZrO_2 samples (Table 1). This is attributed to the agglomeration of platinum oxide species, as well as of cerium oxide phase, being seen from the XRD spectra (Fig. 2B).

Pore size distribution of the samples determined by the Barret–Joyner–Halenda (BJH) method to the desorption branch of the isotherms is shown in Fig. 1. The pore size distribution for Pt/ZrO_2 and Pt/CeO_2–ZrO_2 samples is centred at about 27 nm and is similar to that of pure ZrO_2. The curve of the pore size distribution is more symmetrical for ZrO_2 sample, corresponding to mesoporous material [23]. The curve symmetry deceases slightly with increasing the CeO_2 content.

3.2. X-ray diffraction

The X-ray diffraction patterns of Pt/CeO_2–ZrO_2 samples as well as of Pt/CeO_2 and Pt/ZrO_2, calcined at 773 and 1073 K, are shown in Fig. 2A and B, respectively. All patterns display broad peaks characteristic of zirconia phase, especially at low temperature treatment. Due to the broadness of the diffraction peaks, it is difficult to define by XRD whether zirconia phase is tetragonal or cubic because these crystallographic phases display similar interplanar spacings [26]. Characteristic diffraction lines at $2\theta = 28.5^\circ$, 33.3°, 47.5° and 56.4° of CeO_2 fluorite structure [27] are well defined in the spectrum of Pt/CeO_2 sample after calcination at 773 (Fig. 2A). Similar to the observation for the mixed CeO_2–ZrO_2 oxide [19], the XRD patterns of the sample with the highest CeO_2 loading (12 wt%) shows a slight shift of the main peak from the position, corresponding to ZrO_2 phase, to lower 2θ values (from 30.4° to 30.0°). This is an indication of the enrichment of the zirconia surface with cerium oxide species.

The crystallite size of CeO_2, ZrO_2 and Pt evaluated from the full-width at half maximum (FWHM) of the samples calcined at both temperatures are listed in Table 1. No diffraction peaks of Pt oxide are observed for the samples calcined at 773 (Fig. 2A), which is anticipated due to the low noble metal loading and high dispersion. However, a strong agglomeration of Pt at $2\theta = 39^\circ$ is observed for ZrO_2- and CeO_2–ZrO_2-supported Pt samples after treatment at high temperature of 1073 K (Fig. 2B and Table 1). There is no evidence for the peak corresponding to the Pt sintering on the surface of Pt/CeO_2, probably, due to a strong Pt–CeO_2 interaction. It should be noted that the X-ray profiles of the reduced samples (not shown) did not detected agglomerated Pt that means that Pt particles are well dispersed on the surface of reduced samples. Calcination at high temperature of 1073 K leads to some crystallization of ZrO_2 and more strongly, for CeO_2 (from 9.8 to 16.4 nm for Pt/CeO_2 sample, Table 1 and Fig. 2B).

3.3. Raman spectra

Raman spectroscopy was applied in order to determine the coordination symmetry of the cations in the mixed CeO_2–ZrO_2

Table 1
Textural properties, particle size (d_{XRD}), Raman ratio and H_2 consumption for Pt/CeO_2–ZrO_2 samples.

Sample	S_{BET} (m^2/g)		V_{pore} (cm^3/g	d_{XRD} (nm)		Raman ratio (a.u.)	H_2 consump. ($\mu mol/g_{cat}$)	
	Carriers	Catalysts		ZrO_2	Pt		Carriers	Catalysts
ZrO_2	217	– (190)[a]	0.53 (0.40)[a]	– (7.3)		–	0.87	–
Pt/ZrO_2	–	199 (183)	0.52 (0.40)	5.7 (6.8)[a]	35.0[a]	4.45	–	0.50
$Pt/1CeO_2$–ZrO_2	204	197 (180)	0.49 (0.39)	5.8 (7.0)	34.5	4.42	0.44	0.51
$Pt/3CeO_2$–ZrO_2	194	193 (–)	0.48 (–)	5.6 (6.9)	34.0	4.40	0.45	0.57
$Pt/6CeO_2$–ZrO_2	190	183 (165)	0.47 (0.37)	6.1 (7.1)	28.6	3.17	0.53	0.62
$Pt/12CeO_2$–ZrO_2	180	170 (154)	0.42 (0.32)	6.2 (7.2)	30.5	2.33	0.81	1.25
Pt/CeO_2	65	54 (9.8)	0.05 (0.02)	10 (16.4)[b]	–	–	–	1.02
CeO_2	–	–	–	–	–	–	1.79	–

[a] At 1073 K.
[b] For CeO_2.

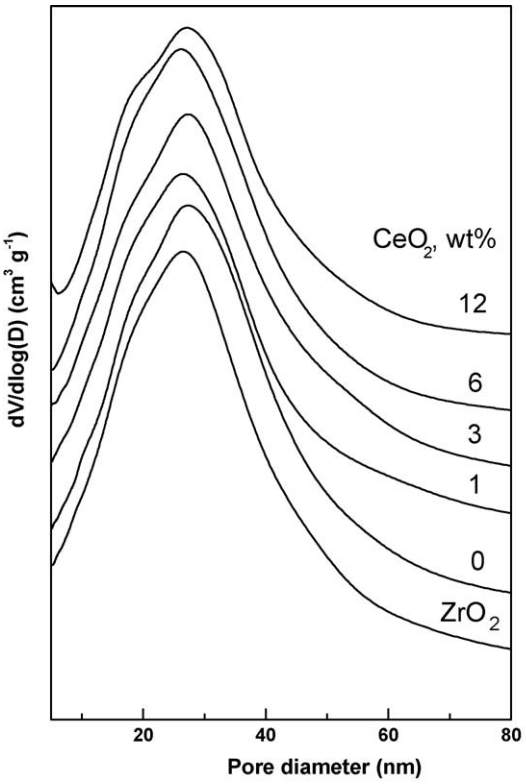

Fig. 1. Pore size distribution for Pt/ZrO_2 and Pt/CeO_2–ZrO_2 samples calcined at 773 K.

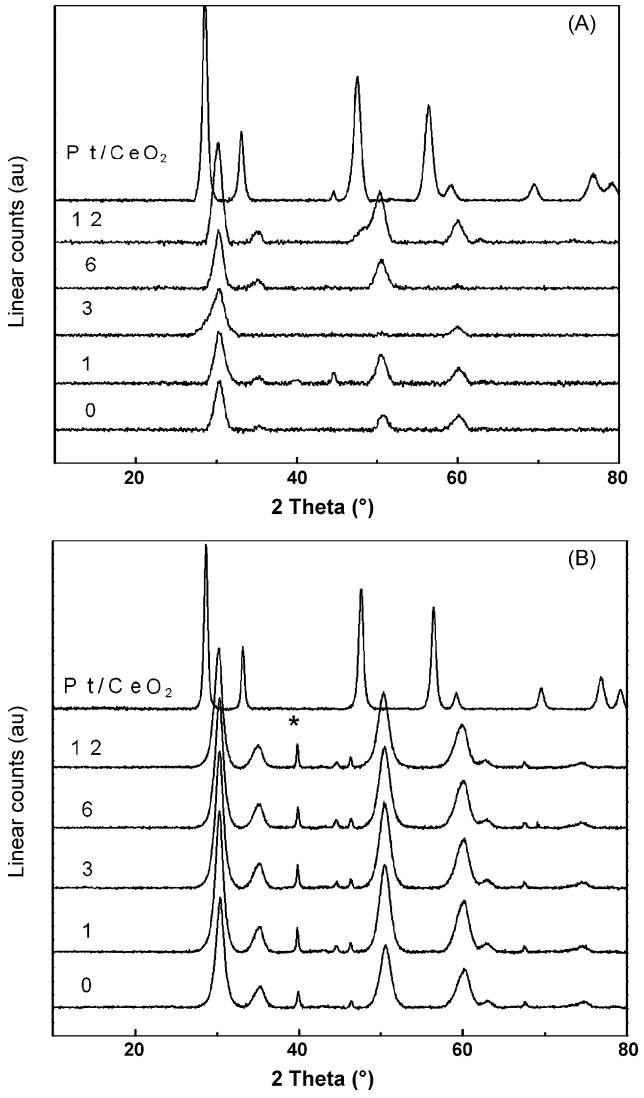

Fig. 2. XRD for Pt/ZrO_2, Pt/CeO_2 and Pt/CeO_2–ZrO_2 samples calcined at 773 K (A) and 1073 K (B); agglomerated Pt*.

oxides. The Raman spectra of supported Pt catalysts calcined at 1073 K are shown in Fig. 3. In the Raman spectrum of pure ZrO_2 broad bands at 148, 262, 307, 439 and 633 cm^{-1} are observed that characterize the tetragonal phase of zirconia [28,29]. Six-Raman-active modes of $A_{1g} + 3E_g + 2B_{1g}$ symmetry are typical for tetragonal ZrO_2 phase (space group $P4_{2/nmc}$) [28,29]. The spectrum of Pt/CeO_2 is mainly constituted by a narrow and slightly asymmetric band at 452 cm^{-1} with faint bands or shoulders being appreciated at ca. 153 cm^{-1} and in the range of 530–580 cm^{-1} (Fig. 3). The main band is related to the first-order peak of F_{2g} symmetry, which is the only allowed Raman mode for fluorite-structured oxides [30]. According to previous detailed analysis of Raman spectra of ceria and doped-ceria samples [31] the asymmetry of the main band and the appearance of other weak bands are caused by the presence of oxygen vacancies defects and lattice strain of CeO_2. The same phenomenon is observed for zirconia-loaded oxides, revealed by broadness of the bands (Fig. 3).

For Pt/CeO_2–ZrO_2 samples the intensity of the band in the region of 400–500 cm^{-1} increases compared to that for Pt/ZrO_2. Also, the position of this band is shifted to a higher wavenumber, near to that for Pt/CeO_2 sample (from 439 to 450 cm^{-1}). It means that this band is an overlapping of the peaks belonging to ZrO_2 and CeO_2 species. In addition the change of the ratio between the relative areas of the bands at 230–360 and 452 cm^{-1} (Table 1) is taken as an indication of the ceria-enriched zirconia surface; the lowest value is detected for the sample with the highest CeO_2 loading (12 wt%).

3.4. XPS analysis

XP spectra of Pt 4f core electrons for fresh reduced Pt/CeO_2–ZrO_2 catalysts are shown in Fig. 4. As seen in this figure, the Pt 4f line profile can be satisfactorily fitted to two doublets whose $Pt4f_{7/2}$ components appear at 71.2 and 72.6 eV. The binding energy value of the Pt $4f_{7/2}$ component at 71.2 eV is characteristic of platinum metal [32]. The binding energy of the second component at 72.6 eV is in between that of Pt^0 and PtO and is associated to partially oxidized platinum surface [33]. For simplicity, the partially oxidized platinum surface is represented by $Pt^{\delta+}$. From the data in Table 2 it is clear that platinum is less oxidized in the catalysts with lower CeO_2 loading (1 and 3 wt%) whereas no Pt^0 at all is detected on the ZrO_2-free catalyst (BE Pt $4f_{7/2}$ = 72.7 eV). This latter finding is not surprising considering the strong metal–support interaction (SMSI) effect developed at the interface between Pt clusters and CeO_2 surface, whose extent enhances upon high-temperature reduction [34]. Indeed, the presence of CeO_2 hinders the complete reduction of platinum clusters. Similar effect of the CeO_2 has been observed for other noble metals, like Rh [13,25]. It is emphasized that platinum appears completely reduced to Pt^0 in the spent catalysts which have been subjected to the conditions imposed by the methane dry reforming reaction, i.e. 823 K. The BE of Zr $3d_{5/2}$ core electrons for all samples is constant (182.2 eV). This value fits well will literature reports for bulk zirconia [35] and is somewhat lower than compared to that of non-treated ZrO_2 (≈183 eV) [36]. Neither traces of chlorine nor alkaline elements were detected.

Fig. 5 shows X-ray photoelectron spectra of Ce $3d_{5/2}$ and Ce $3d_{3/2}$ core levels for all H_2-reduced samples. According to the notation

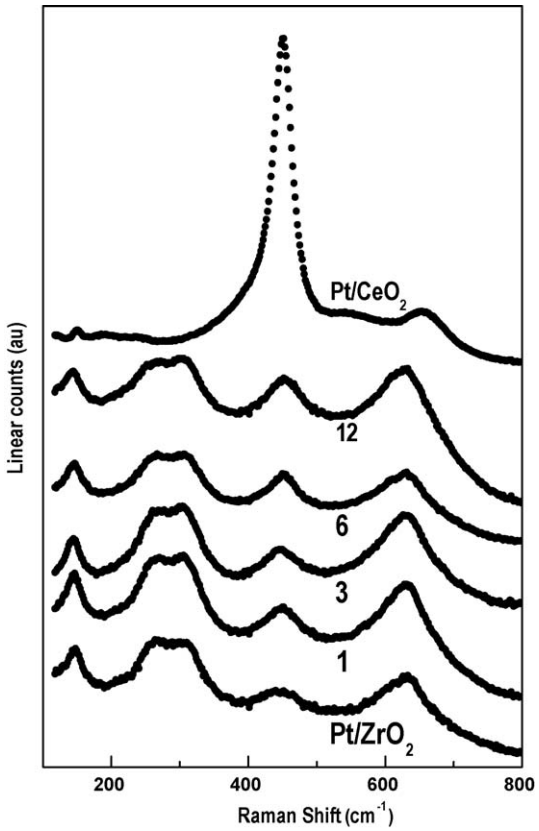

Fig. 3. Raman spectra for Pt/ZrO_2, Pt/CeO_2 and Pt/CeO_2–ZrO_2 samples calcined at 1073 K.

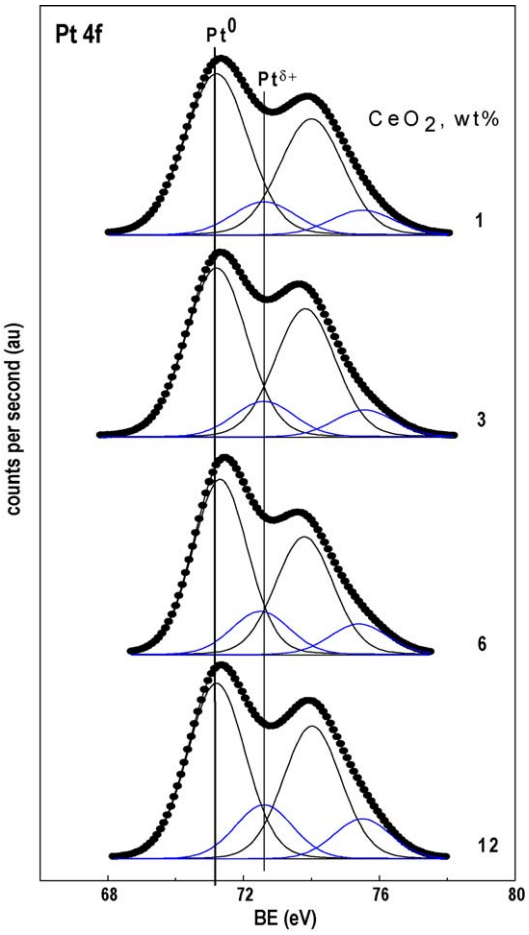

Fig. 4. XPS of Pt 4f region for reduced Pt/ZrO_2, Pt/CeO_2 and Pt/CeO_2–ZrO_2 samples.

proposed by Burroughs et al. [37], the $3d_{3/2}$ multiplet signals of Ce(IV) are labelled U, U″ and U‴, whereas those of $3d_{5/2}$ are labelled V, V′ and V″. The Ce(III) signal exhibits only four peaks (U_0, U′, V_0 and V′). Accordingly, the catalyst containing 1–12 wt% CeO_2 containing both Ce(IV) and Ce (III) species, however the Ce 3d spectrum of ZrO_2-free sample is dominated by the Ce(IV) features, for which the binding energy of the Ce $3d_{5/2}$ peak (882.8 eV) corresponds to CeO_2 [12,38]. A quantitative estimation of the Ce(IV) concentration at the surface of CeO_2–ZrO_2 samples can be performed based on the ratio between the integrated intensity of the well resolved satellite peak U‴ at around 916.5 eV and the total area of the Ce 3d energy region (main Ce3d peaks and satellites) [12,39]. The value of this ratio ($I_{U'''}/I_T$) is 0.15 for the ZrO_2-free sample, which is very close to the value usually found in pure CeO_2 ($I_{U'''}/I_T$ = 0.16). Notwithstanding, for the H_2-reduced 1, 3, 6 and 12 wt% CeO_2 containing catalysts the values of the $I_{U'''}/I_T$ ratio are 0.03, 0.03, 0.02 and 0.06, respectively. This semi-quantitative estimate indicates clearly that cerium is essentially as Ce(III), and most specifically in the region of lowest Ce-loadings. It can be concluded that both $Pt^0/Pt^{\delta+}$ and Ce^{3+}/Ce^{4+} redox couples really exist over Pt/CeO_2–ZrO_2 samples under reduction atmosphere.

The relative percentages of platinum and cerium relative to zirconium (Pt/Zr and Ce/Zr) were calculated from the intensity ratios (I_{Pt4f}/I_{Zr3d} and I_{Ce3d}/I_{Zr3d}) normalized by atomic sensitivity factors [40]. These ratios are listed in Table 2. It can be seen that the

Table 2
Binding energies (eV) and surface atomic ratios for reduced and spent Pt/CeO_2–ZrO_2 catalysts.

Sample	Zr $3d_{5/2}$	Ce $3d_{5/2}$	Pt $4f_{7/2}$		Ce/Zr	Pt/Zr
$Pt/1CeO_2$–ZrO_2	182.1	882.4	71.2 (83)[a]	72.6 (17)[b]	0.007 (0.01)	0.008
	182.2		*71.0*		*0.010*	*0.005*
$Pt/3CeO_2$–ZrO_2	182.1		71.2 (83)	72.6 (17)	0.013 (0.03)	0.007
	182.2	882.3	*71.0*		*0.011*	*0.004*
$Pt/6CeO_2$–ZrO_2	182.1		71.3 (80)	72.5 (20)	0.034 (0.06)	0.007
	182.2	882.2	*71.1*		*0.028*	*0.005*
$Pt/12CeO_2$–ZrO_2	182.2	882.4	71.2 (76)	72.6 (24)	0.081 (0.12)	0.008
	182.2	881.8	*71.1* (*100*)		*0.047*	*0.006*
Pt/ZrO_2	182.2	–	71.2 (100)			0.010
	182.2		*71.1* (*100*)		–	*0.006*
Pt/CeO_2		882.8	72.7 (100)			Pt/Ce = 0.028
	–	*882.0*	*71.0* (*100*)		–	Pt/Ce = *0.023*

BEs values and surface atomic ratios for spent catalysts are in italic.
[a] Pt^0.
[b] $Pt^{\delta+}$.

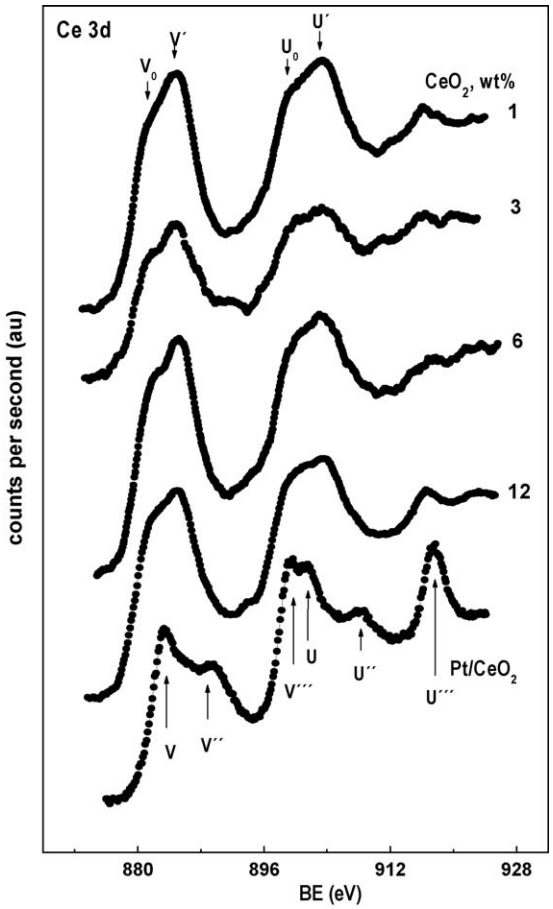

Fig. 5. XPS of Ce 3d region for reduced Pt/CeO_2 and Pt/CeO_2–ZrO_2 samples.

Ce/Zr ratios are somewhat lower than that the nominal ones (values in parenthesis in the column of Ce/Zr ratios in Table 2). This suggests that the surface is slightly Ce-impoverished very likely as a consequence of formation of very small clusters of CeO_2. Indeed, the X-ray diffraction pattern of the 12 wt% CeO_2-containing sample displayed a splitting of the peaks at 50.4° and 48.6° which is consistent with CeO_2 segregation. Unfortunately, due to the line broadening in the other samples containing 1–6 wt% CeO_2, X-ray analysis does not provide additional information, however the very high surface sensitivity of XPS technique allows precisely quantifying the CeO_2 segregation.

The XP spectra of Ce 3d core-level of spent catalysts were also recorded (no reported for sake of simplicity) and BEs values of core electrons and surface atomic ratios are also compiled in Table 2. The Ce 3d line profile of 1–12 wt% CeO_2 loaded samples displayed only the four peaks U_0, U′, V_0 and V′, indicating that all cerium atoms became completely reduced to Ce(III) during on-stream. However, no reduction is visible in the spent Pt/CeO_2 catalyst as confirmed by the value of $I_{U'''}/I_T$ ratio of 0.16.

The Pt/Zr ratios for the 1–12 wt% CeO_2-containing samples are similar to that of the cerium-free sample. Although this finding might suggest that platinum nanoparticles distribute randomly between the Zr–Ce–O phase and CeO_2 clusters, preferential interaction between Pt and CeO_2 phase can occur. In the Pt/CeO_2–Al_2O_3 system, it has been shown [8,34] that Pt interacts preferentially with Ce even in the presence of a much larger Al_2O_3 surface. The value of Pt/Ce ratio for Pt/CeO_2 sample is almost three times higher than that of Pt/Zr for Pt/ZrO_2, which would be taken as better exposure of Pt atoms on ceria surface. However, taking into account that specific BET area of ZrO_2 is almost three fold that of CeO_2, it appears that the same increase runs in parallel with the Pt 4f XPS signal. Thus, platinum exposure (or dispersion) virtually coincides in ZrO_2 and CeO_2 substrates.

For the spent catalysts, both Pt/Zr and Ce/Zr surface atomic ratios decrease with respect the H_2-reduced counterparts (Table 2). Thermally induced sintering of platinum and ceria phases and partial coverage of these phases by carbonaceous deposits would be responsible for such a drop. The data from Table 2 shows a strong sintering of ceria phase for Pt/CeO_2–ZrO_2 sample with the highest CeO_2 loading (12 wt%); the Ce/Zr ratio decreases from 0.081 to 0.047 for reduced and spent catalyst, respectively. No significant change in the Ce/Zr ratio should be expected due to its thermal stabilization in air for samples with lower CeO_2 (1–3 wt%) [19] caused by the strong interaction between Ce and Zr, as well as between Ce and Pt. On other hand, the decrease of atomic ratios for spent catalysts would be caused by the formation of carbonaceous patches on the metal and substrate (Zr–Ce–O) surfaces.

3.5. TPR

3.5.1. CeO_2–ZrO_2 samples

Evaluation of the reducibility of the support is very important issue in connection with its ability to generate oxygen vacancies and to transfer the oxygen into the metal particle. TPR profiles of CeO_2, ZrO_2 and CeO_2–ZrO_2 oxides are shown in Fig. 6A. The calculated hydrogen consumption for CeO_2–ZrO_2 oxides and Pt/CeO_2–ZrO_2 samples is presented in Table 1. The TPR of bulk CeO_2 exhibits two broad intense peaks: the first one at 785 K and the second one at 1077 K (Fig. 6A). The TPR profile of CeO_2 can be interpreted as a stepwise reduction of CeO_2 [8]. The first peak is due to the surface shell reduction of ceria whereas the second one is attributed to the total reduction of ceria by elimination of O^{2-} anions of the lattice and formation of Ce_2O_3 [8]. The highest H_2 consumption is observed for bulk CeO_2 (Table 1).

Upon reduction, bulk zirconia exhibits a broad H_2 uptake with ill-resolved maxima at 856 and 908 K (Fig. 6). The observed reducibility of ZrO_2 is unusual since no reduction of ZrO_2 was observed in many reports. Most likely, this reduction depends on the kind of zirconia phase, as well as on the method of preparation. Similar feature for ZrO_2 under reduction conditions has been reported [41]. The reduction process can involve both the surface carbonate decomposition and the uptake of hydrogen during formation of the type II bridging OH groups (surface shell reduction) [41]. Since no carbonate formation was detected, it can be assumed that the H_2 uptake for ZrO_2 is mainly caused by the formation of surface bridging OH bonds.

The TPR profiles of the mixed CeO_2–ZrO_2 oxides with different CeO_2 loading differ from those of the bulk oxides (Fig. 6A). The TPR patterns change with the increasing CeO_2 content: (i) the main peak maximum temperature is shifted to lower values (from 853 to 834 K for 1 and 12 wt% CeO_2); and (ii) a small peak at about 717 K appeared at $CeO_2 \geq 6$ wt%. The temperature peak of 717 K can be related to the reduction of deposited cerium oxide species on zirconia surface. The main TPR peak for CeO_2–ZrO_2 samples overlaps with that of the reduction of CeO_2 particles and the surface shell reduction of ZrO_2. The shift of the main TPR peak to low temperature, probably is favoured by the highly oxygen mobility on zirconia surface after incorporation of cerium atoms into ZrO_2 similar to CeO_2–ZrO_2 solid solution formation [42]. In the higher temperature region of the TPR of the sample with the highest CeO_2 loading the small peak at about 1088 K would be attributed to the formation of Ce_2O_3 caused by the bulk reduction of CeO_2 [8] (Fig. 6A). The calculated H_2 consumption for CeO_2–ZrO_2 oxides slightly increases with the increasing CeO_2 content (Table 1).

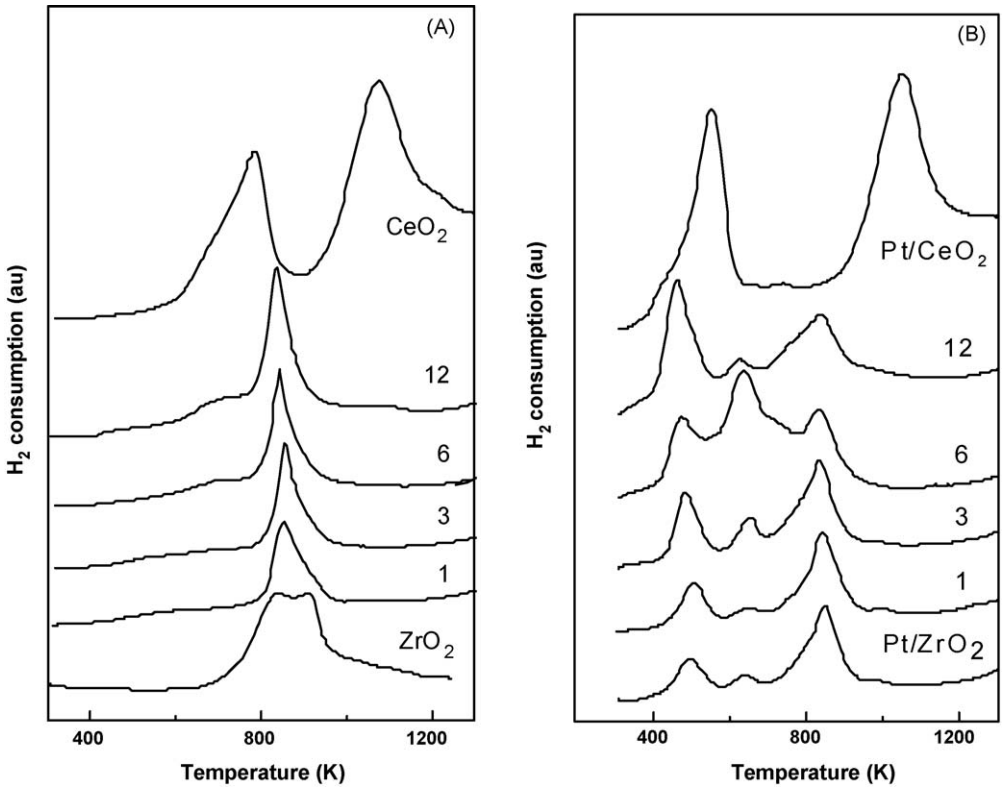

Fig. 6. TPR for bulk ZrO_2 and CeO_2 and CeO_2–ZrO_2 oxides (A) and Pt/ZrO_2, Pt/CeO_2 and Pt/CeO_2–ZrO_2 catalysts (B).

3.5.2. Pt/CeO_2–ZrO_2

The TPR profiles of CeO_2–ZrO_2-supported Pt catalysts (Fig. 6B) differ with respect those of the bulk CeO_2 and ZrO_2 and mixed CeO_2–ZrO_2 oxides (Fig. 6A). In addition, the values of the consumed hydrogen of supported Pt catalysts are higher compared to those of the corresponding carriers (Table 1). This difference is due to the type and the strength of the interaction between supported platinum oxide species and support. To facilitate the description of the TPR profiles of the Pt/CeO_2–ZrO_2 samples, the TPR patterns are divided in three temperature regions: region I (420–550 K), region II (600–700 K) and region III (720–900 K). The regions I and II should be related to the reduction of supported Pt oxide species and to the reduction of the sum of platinum and cerium oxide species, respectively. The intense peak in all TPR profiles (the third region) is due to the reduction of surface shell reduction of zirconia, as well as of CeO_2. The position and the relative intensities of the peaks strongly depend on the CeO_2 content.

The TPR profile of Pt/CeO_2 shows two strong peaks at 553 and 1053 K associated with the surface and bulk reduction of CeO_2, respectively [42]. The maximum of the first peak is placed at significantly lower temperatures than that of the bulk CeO_2 (Fig. 6). This is in agreement with other studies [43], which have shown that the presence of noble metal can facilitate the reducibility of the support surface. However, the maximum of the second peak is affected only slightly in the presence of Pt. It means that the deposition of Pt on the surface of ceria has a little effect on the bulk reduction of CeO_2. This observation was interpreted in terms of kinetic model [44], which assumes that the high-temperature reduction process is controlled by the slow bulk diffusion of the oxygen vacancies created at the oxide surface. This leads to an increase of the oxygen exchange capacity of CeO_2 due to the noble metal–CeO_2 interaction. This behaviour was generally explained by the hydrogen *spill over* effect, which takes place from the metallic Pt. On the other hand, ceria can lead to a decrease of the reduction temperature of platinum oxide species. In the past [8,45], it has been observed that the reduction of Pt oxide occurs first at a slightly lower temperature than that of the CeO_2 surface shell reduction. Therefore, the lower temperature shoulder at about 442 K in Fig. 6B is most likely associated with the reduction of Pt to Pt^0, while the most intense peak is due to the reduction of the ceria surface shell. This occurs either via oxygen vacancy formation and subsequent dissociation of H_2O to form bridging OH groups, or direct H_2 dissociation and *spill over* to the ceria surface. The presence of large platinum oxide crystallites cannot be precluded because of the low surface area of CeO_2 (Table 1).

The lowest temperature peak at 496 K in the TPR profile of Pt/ZrO_2 (Fig. 6B) would be ascribed to a reduction of Pt oxide species in isolated patches and/or to a reduction of oxychlorplatinum surface complex, $[PtO_xCl_y]_s$ to metallic Pt [46]. The small peak at 635 K could be assigned to a reduction of well-dispersed platinum oxide species in some interaction with the surface of ZrO_2 (PtO_x–ZrO_2 species). The incorporation of Pt to ZrO_2 shifts the TPR peak from the surface shell reduction of the support to a lower temperature, but not too strong as in the case of Pt/CeO_2. Recently it has been reported [41] that the defects (e.g. vacancies) in the surface of zirconia could be generated with the presence of Pt that can be involved in the catalysts of dry reforming.

Similar to the CeO_2–ZrO_2 oxides, the same trend in the change of hydrogen consumption with the increase of CeO_2 content is observed for supported Pt catalysts (Table 1). Addition of a small amount of CeO_2 (1–3 wt%) into Pt/CeO_2–ZrO_2 samples causes a slight shift of the maximum of the second TPR peak to higher temperatures relative to that of Pt/ZrO_2 (from 635 to 649 and 658 K, respectively). This suggests a strong interaction between platinum and cerium-modified zirconia formed during preparation of the samples. Increasing the CeO_2 content leads to systematic shifts in the temperature of reduction of Pt to Pt^0 to lower values (from 508 to 462 K for 1 and 12 wt% CeO_2, respectively). For the peak associated with PtO_x–ZrO_2 interacting species there is also a shift to lower temperature (628 K). A similar behaviour was

reported previously [47]. It should be noted that the hydrogen uptake for the peak at 462 K for the sample with 12 wt% CeO_2 is much larger than expected for the reduction of all platinum. This peak is likely due to the reduction of platinum oxide species and synergistically reduced ceria agglomerates. This was attributed to the ability of supported metal to activate H_2 and then to spill it onto the support inducing a concurrent reduction of both the platinum oxide and the surface of the support [48]. The hydrogen uptake is increased for high CeO_2-loaded samples (Fig. 6B and Table 1).

On the other hand, the surface reduction of zirconia is promoted by the presence of Pt as well as of ceria, which is revealed by continually broadening of the left side of the highest temperature peak at about 841 K with the increase of CeO_2 content in Pt/CeO_2–ZrO_2 samples. For ceria-rich samples there is some overlapping of the peaks due to the reduction of ceria and zirconia. It is not surprising the high intensity of the peak at 635 K compared to other peaks in the TPR profile of the sample with 6 wt% CeO_2 (Fig. 6B). This peak would be composed of the subsequent reduction of well-dispersed CeO_2 crystallites due to the spillover of platinum plus the reduction of PtO_x species in direct contact with the support surface. Since Pt–CeO_2 interaction is already evident for Pt/CeO_2 sample, it is apparent that Pt interacts preferentially with ceria in the presence of much larger zirconia surface. As the CeO_2 concentration is increased, the surface of zirconia becomes saturated with well-dispersed CeO_2 particles and the peak at 635 K is bigger for catalyst with 6 wt% CeO_2. In opposite to that, the surface of CeO_2-rich sample (12 wt%) is covered with agglomerated CeO_2 crystallite that causes the surface of ZrO_2 to be freer. The maximum of the TPR peak for $Pt/12CeO_2$–ZrO_2 due to the reduction of PtO_x–ZrO_2 species is near to that for Pt/ZrO_2.

3.6. Thermogravimetric analysis

TG curves of the spent catalysts (not shown) demonstrated that during the heating ramp, starting from 300 to 1000 K, a weight loss was observed up to 423 K that would be connected with the removal of water. There was a new weight loss in the temperature range of 440–523 K. The overall weight loss would correspond to the sum of oxidation of carbonaceous species and oxidation of the reduced cerium and platinum. The decrease in the weight loss for the samples followed the order: $Pt/6CeO_2$–$ZrO_2 \approx Pt/12CeO_2$–$ZrO_2 \approx Pt/ZrO_2 > Pt/1CeO_2$–$ZrO_2 > Pt/CeO_2$. It is seen that there is no a linear correlation between the amount of the weight loss and CeO_2 content. The lowest weight loss was observed for Pt/CeO_2 catalyst.

DTA analysis of the spent catalysts is presented in Fig. 7. It is seen that the temperature of coke combustion as well the intensity of evaluated CO_2 peak is lower for Pt/CeO_2 catalyst compared to those for other samples. This coincides with the lowest weight loss of this catalyst. It can be concluded that the ability of the catalysts to eliminate the carbon is high for CeO_2-supported Pt catalyst.

3.7. Catalytic performance

The evolution of CH_4 and CO_2 conversions, as well as the yield of H_2 and CO with time on-stream for Pt catalysts supported on mixed CeO_2–ZrO_2 oxides, zirconia and ceria in the reaction of CO_2 reforming of CH_4 at reaction temperature of 823 K are plotted in Fig. 8. Table 3 summarizes the values of CH_4 and CO_2 conversions, H_2 and CO yields, as well as of H_2/CO ratios of some catalysts; the data in Table 3 are taken at steady-state activity and at a reaction temperature of 823 K. It is seen that the CH_4 conversions decrease slightly with the increase of CeO_2 content. The activity of Pt catalysts supported on mixed CeO_2–ZrO_2 is developed with time on-stream and steady-state activity is occurred nearly after 2 h on-stream (Fig. 8). Pt/ZrO_2 catalyst is activated more rapidly, but after few hours in reaction it became slowly deactivated, due mainly to

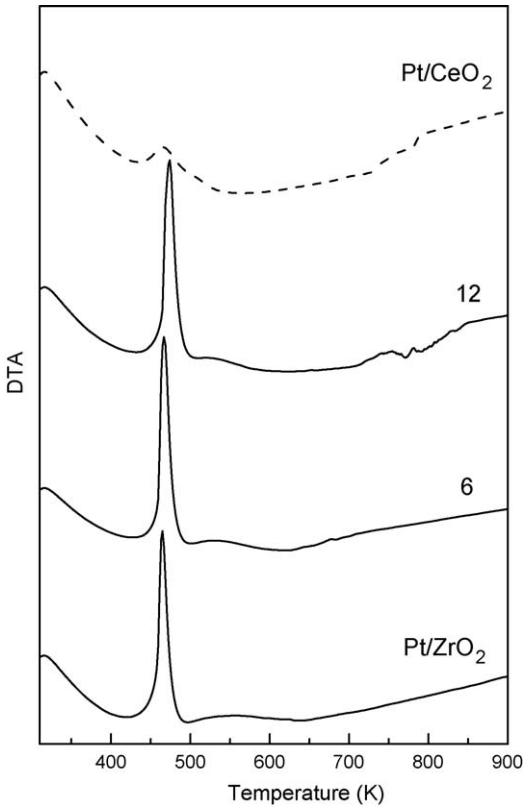

Fig. 7. DTA for spent Pt/ZrO_2, Pt/CeO_2 and some Pt/CeO_2–ZrO_2 catalysts.

formation of coke residues on the catalyst along the test. Pt/CeO_2 catalyst has initial high activity that decreases continuously with time on-stream. The relatively low activity of Pt/CeO_2 can be attributed to its much lower surface area than that of ZrO_2-containing catalysts and to the agglomeration of the CeO_2 phase under reaction conditions. It should be noted that the CO yield is higher for Pt/ZrO_2 and CeO_2-rich Pt/CeO_2–ZrO_2 samples.

From Table 3, it is clear that the H_2/CO ratio in the product stream is not one as expected from the stoichiometric reforming reaction. This is not surprising considering that thermodynamics predicts a H_2/CO ratio of unity only at temperatures above 1073 K [1]. This is a consequence of involvement of the reverse of water gas-shift (RWGS) reaction. Considering the CO_2 reforming of CH_4 (Eq. (5)), influenced by the simultaneous occurrence of the RWGS reaction (Eq. (6)) [1], it is expected that CH_4 conversion is lower than CO_2 conversion:

$$CH_4 + CO_2 \leftrightarrow 2H_2 + 2CO \quad (5)$$

$$CO_2 + H_2 \leftrightarrow CO + H_2O \quad (6)$$

Considering the CeO_2 content in supported Pt catalysts, the order of activity, expressed as CH_4 conversion, decreases in the following order: $Pt/ZrO_2 > Pt/1CeO_2$–$ZrO_2 \approx Pt/3CeO_2$–$ZrO_2 > Pt/6CeO_2$–$ZrO_2 > Pt/12CeO_2$–$ZrO_2 > Pt/CeO_2$. It is clear that zirconia-supported Pt

Table 3
Catalytic behaviours of supported Pt catalysts at T_r = 823 K.

Sample	CH_4 (%)	CO_2 (%)	H_2 yield	CO yield	H_2/CO
Pt/ZrO_2	24.5	25.5	10.2	26.8	0.51
$Pt/1CeO_2$–ZrO_2	20.1	21.0	8.5	23.9	0.48
$Pt/6CeO_2$–ZrO_2	18.0	24.8	9.2	26.1	0.49
$Pt/12CeO_2$–ZrO_2	16.0	23.1	8.8	25.0	0.47
Pt/CeO_2	7.0	12.2	5.5	16.1	0.40

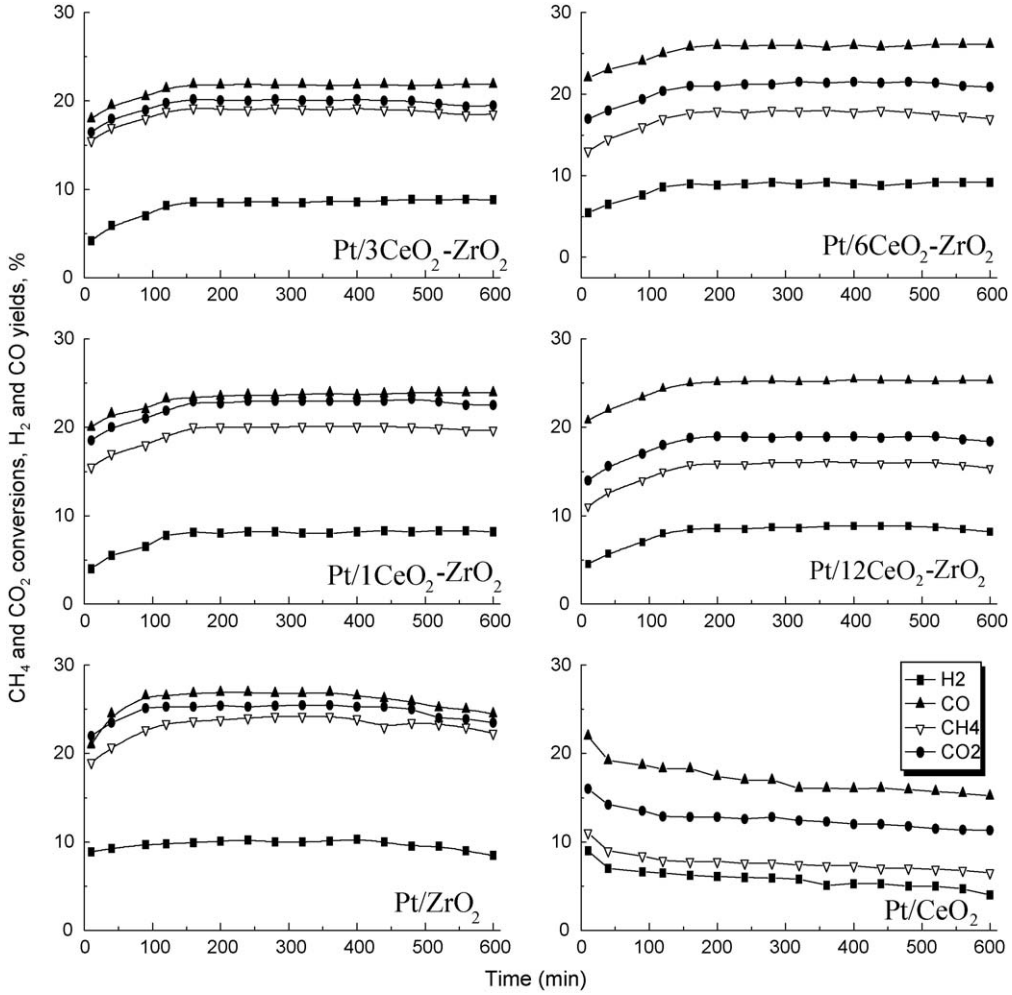

Fig. 8. Evolution of the CH_4 and CO_2 conversions, as well as of H_2 and CO yields for Pt/ZrO_2, Pt/CeO_2 and Pt/CeO_2–ZrO_2 catalysts in the reaction of dry reforming of CH_4 with time on stream at T_r = 823 K.

catalyst has the highest activity. However, it is interesting to note that Pt/ZrO_2 and low CeO_2-loaded catalysts show almost similar CH_4 and CO_2 conversions. Probably, other parasite reactions occur, like methanation of CO_2 to CH_4 [1] in parallel with RWGS. An increase of the values of CO_2 conversion compared to those of CH_4 conversion is more evident for high CeO_2-loaded Pt catalysts, as well as for Pt/CeO_2. This means that CeO_2 promotes the CO_2 activation. The yield amounts of H_2 and CO decrease slightly after addition of a small amount of CeO_2 and then increase again for CeO_2-reach catalysts. The minimum amounts of H_2 and CO are produced for Pt/CeO_2 catalyst contrary to that observed for Pt/ZrO_2 (Table 3). The results differ from previous studies [49,50]. It has been observed a much higher activity and stability for Pt catalysts supported on ceria-promoted zirconia compared to those CeO_2-free Pt/ZrO_2 catalyst [49,50]. The latter would be connected with the kind of zirconia support.

Fig. 8 demonstrates clearly that the Pt/CeO_2–ZrO_2 catalysts are stable in the reaction of reforming of methane with CO_2. It is well known that the clean ability of the catalysts depends on the kind of deposited carbon and/or on the location of the carbon on the catalyst surface.

4. Discussion

4.1. Structural and surface features of Pt/CeO_2–ZrO_2 catalysts

An increase of the Ce/Zr ratio indicates a higher fraction of cerium species on the surface. However, an interesting trend appears. Table 2 shows that the Ce/Zr ratio for the sample with the lowest CeO_2 content is very high. Since the influence of Zr oscillations or the Pt percentage on the amounts of surface Ce atoms is negligible, the Ce/Zr ratio is mainly determined by the change of the CeO_2 content. This would be an indication of high cerium dispersion on the surface of zirconia caused by an interaction between cerium and zirconium species stabilizing cerium in a lower oxidation state (Fig. 5). It would be proposed that Ce at low contents is atomically dispersed on zirconia and the ionic state of cerium is far from Ce^{4+} (Fig. 5 and Table 2). The same effect has been observed for other systems, like ZrO_2 (CeO_2)–Al_2O_3 (SiO_2) [27,36]. Well-dispersed CeO_2 crystallites are another cerium oxide species on zirconia, but they have very small size. The small crystallite nature of these cerium oxide species is supported by the lack of XRD characteristic of bulk CeO_2 (smaller than 4 nm) and quantitative XPS data. Finally, at high CeO_2 content (12 wt%) large CeO_2 particles are accumulated on zirconia surface, being observed by XRD.

XRD, XPS and TPR results show clearly that the pre-treatment temperature and the type of the support influence significantly on the morphology of Pt particles in the oxidic, as well as in the reduced samples. Pt–Ce and Ce–Zr interactions can affect either the degree of Pt sintering during calcination or the ability of Pt to adsorb hydrogen under reductive atmosphere. In the fresh samples it would be concluded that Pt is well dispersed on the surface of zirconia and mixed CeO_2–ZrO_2 oxides. It is well known the influence of CeO_2 on the increase of the dispersion of the noble

metal over different supports and to prevent the agglomeration of dispersed Pt into discrete particles [27,36]. The extensive sintering of Pt is observed on zirconia and CeO_2–ZrO_2 oxides after pre-treatment in an oxidizing environment at 1073 K (Table 1). The increase of CeO_2 content leads to decrease of Pt sintering (Table 1). Agglomeration of Pt on pure CeO_2 did not occur being confirmed by XRD. However, it cannot be excluded the formation of bigger Pt oxide species on the surface of bulk CeO_2 due to its low surface area. As it was discussed previously in our work [27], the main reason for Pt sintering would be the thermal decomposition of the surface complex $[PtO_xCl_y]_x$ to Pt atoms or small clusters that rapidly migrate to the surface and via nucleation mechanism metallic crystallites are formed. It has been shown [46] that in the temperature region of 973–1173 K there is a bimodal distribution of Pt between relatively large crystals and molecular dispersed surface species. It is important to note, that after treatment of the samples under reductive atmosphere there was not Pt sintering. Therefore, it is expected that a strong Pt sintering does not occur during reforming reaction. The stabilization of $Pt^{\delta+}$ species after hydrogen treatment of Pt/CeO_2–ZrO_2 catalysts (Table 2) means a strong interaction between Pt and Ce. Thus, a high dispersion of Pt can be favoured by the presence of cerium.

4.2. Catalytic behaviour of Pt/CeO_2–ZrO_2

Comparing the activity of the catalysts related to CH_4 and CO_2 conversions it could be assumed that the methane and CO_2 activation and decomposition should be dominant on the metallic Pt supported on ZrO_2. The CH_4 conversions of the catalysts decrease with increasing CeO_2 content. This would be connected with the differences in the number of accessible active metal surface sites on the catalyst surface. The lowest activity of Pt/CeO_2 is caused by the lowest surface area of the catalyst. The effect of the CeO_2 addition to Pt/ZrO_2 catalyst can be related to the existence of a strong interaction between platinum and cerium. The TPR and XPS results of reduced samples demonstrate that this interaction can result in an increase of the amount of partially reduced Pt sites ($Pt^{\delta+}$, where $0 < \delta < 1$) in the catalysts with a higher CeO_2 content ($\geq$6 wt%) due to a strong interaction between deposited metal particles and CeO_2 modified support.

The strong metal–support interaction has been intensively investigated in ceria- and other oxide-supported noble metal catalysts by many authors [1,51–53]. In the SMSI state, Pt is decorated by the partially reduced oxide suppressing the hydrogen chemisorption capacity, but leaving the particle size unaffected. This process can be reversed by O_2 or water as was suggested by Bitter et al. [53]. It was proposed that during reaction conditions the SMSI state is absent, since it was possible CO_2 to be dissociated on the catalyst to CO and O_{ads} shown by IR spectroscopy [53]. The O_{ads} was responsible for oxidizing the ZrO_x species on the Pt and, thus minimizing the extent of decoration with oxides islands [48]. However, in our case this interaction is not the SMSI, operated by covering the transition metal with reduced support species. It has been demonstrated [51] by HRTEM that the metal decoration effect occurs on Pt/CeO_2 at reduction temperature higher than 773 K. We would propose that the nature of this Pt–CeO_2 interaction is electronic, involving a charge transfer between Pt and neighbouring CeO_2 and/or ZrO_2 particles similar to the observations for CeO_2–Al_2O_3-supported Pt [8] and Rh catalysts [13].

Different results regarding the active sites of the noble metal for CO_2 reforming of methane have been proposed. Some studies claim that metallic Pt sites are the most active sites [8,12,54], while other propose a more complex structure with the noble metal of different oxidation state present on the surface [13,25]. The high CH_4 dissociation over Rh/CeO_2–Al_2O_3 catalysts was related to the presence of partially oxidized $Rh^{\delta+}$ species that was connected with its ability to accept σ electrons of methane molecule [13,25].

The enhanced CH_4 conversion of Pt/ZrO_2 (Table 2) can be related mainly to the presence of fully reduced platinum and its high dispersion on zirconia surface. Pt is more easily reduced on zirconia surface and, practically, all platinum is in Pt^0 state as was detected by XPS. However, the activity begins to drop slowly with time on stream (Fig. 9) due to the agglomeration of Pt under reaction conditions (Table 2). Addition of a small amount of CeO_2 (1–3 wt%) to zirconia leads to a decrease of the yield amounts of H_2 and CO compared to that of Pt/ZrO_2 catalyst and after that, they increase again for CeO_2-rich samples (Table 3). The same trend is observed for the change of CO_2 conversions. The lowest H_2 and CO yields as well as the lowest CH_4 and CO_2 conversions are detected for Pt/CeO_2 that could be connected with the smallest surface area of the ceria carrier causing the agglomeration of Pt particles. Therefore, the number of accessible metallic active sites is decreased. Therefore, there is a relation between accessible metal Pt area and the activity of the catalysts.

The main reason for decreasing CO_2 conversion after adding small amounts of CeO_2 could be the presence of atomically dispersed cerium that disrupt the interaction between Pt and zirconia support at the metal–support interface and/or the decrease of oxygen vacancies on zirconia surface. Atomically dispersed cerium on the surface of ZrO_2 was observed for calcined CeO_2–ZrO_2 oxides [19] due to the strong interaction between Ce and Zr at low CeO_2 content. The close contact between Pt and Ce for Pt/CeO_2–ZrO_2 catalysts with 1–3 wt% CeO_2, revealed by the highest surface Pt/Ce ratio (Table 2), can be responsible for the low CO_2 conversion (Table 3). The increase of CeO_2 content leads again to acceleration of CO_2 dissociation due to the high capacity of the ceria lattice to dissociate CO_2 molecule [46].

As it is seen in Table 3, the high CH_4 conversion for Pt/ZrO_2 catalysts coincides with a high CO production. One of the ways for increasing the CO yield is the dissociation of CO_2. It has been shown that the CO_2 dissociation proceeds completely differently over Pt/ZrO_2 compared to that over Pt/Al_2O_3 [47]. It involves an oxygen vacancy at zirconia surface and these species are located at the Pt/zirconia interface [53,55] and therefore, the activity is correlated to the available Pt–ZrO_2 perimeter. Efstathiou et al. [56] suggested the participation of zirconia lattice oxygen and lattice vacancies. However, our results suggest that these species are confined to the surface region only as the TPR results revealed a high H_2 uptake from the surface shell reduction of zirconia [19]. These oxygen surface species can be replenished either by CO_2 or by O_2, as has been demonstrated by pre-treating the catalyst with a CO_2 and $^{18}O_2$ mixture [56]. It has been demonstrated that storage of CO and CO_2 on the zirconia surface [53,55], that leads to the formation of formate and carbonate species, respectively, and the carbonate species decompose easily into CO over Zr vacancies when are available. In general, some authors have suggested [53] that catalysts which could form carbonates on the support, like TiO_2, Al_2O_3 and ZrO_2, showed a much higher activity in CO_2/CH_4 reforming reaction compared to those which could not form carbonates (SiO_2). On the other hand, the higher CO yields can be related to the dissociation of CH_4 to H_2 and surface carbon species; the latter react rapidly with the surface oxygen species producing CO [53,56].

There is a change in the values of CH_4 and CO_2 conversions with increasing CeO_2 content ($\geq$6 wt%); the values of CO_2 conversions become higher relative to those of CH_4 in comparison to those for Pt/ZrO_2 and low CeO_2-containing catalysts. It means that the RWGS reaction and/or the dissociation of CO_2 dominate the CH_4 decomposition. Since the water was negligible, contribution of the RWGS appears irrelevant, this would be mainly related to the increase of the oxygen vacancies from CeO_2, promoting the CO_2

dissociation [51]. It is generally accepted that the methane molecule is activated on metallic surfaces [1,8,12,54]. The change of Pt dispersion in CeO_2-containing catalysts (Table 2, Pt/Ce ratios) leads to a change of the number of the active metallic sites for decomposition of CH_4. On the other hand, enrichment of the catalyst surface with CeO_2 activates the dissociation of CO_2 by the mechanism like that for Pt/ZrO_2 catalyst and the CO yields increase for ceria-rich samples (Table 3). The results suggest that the reaction takes place at the interface Pt and support.

The peak of CO_2 evolving from Pt/ZrO_2 (Fig. 8) is symmetric and indicates that it originates from one type of coke. Based on the observations in the literature [54,55] two types of coke by TPO after reforming on Pt/Al_2O_3 were identified: a more reactive carbon attributed to coke on Pt and a less reactive carbon on the support formed by Lewis acid catalyzed decomposition of methane. In the case of Pt/ZrO_2, the absence of appreciable amounts of acid sites on zirconia results in Pt being the dominant sites for coke formation [53,54]. It should be noted that the Pt/ZrO_2 and Pt/CeO_2–ZrO_2 samples have lower H_2 consumption compared to that of Pt/CeO_2 (Table 1). Therefore the CO_2 peak observed for the catalysts would mainly result from oxidizing coke on Pt particles. A high stability for Pt/CeO_2–ZrO_2 catalysts has been observed recently [49] that was related to the higher CO_2 adsorption capacity on CeO_2, which increases the dissociation and cleaning ability. Although the formation of carbon deposits on Pt particles is occurring during the reforming reaction, the catalysts are not deactivated with time on stream. It was proposed [57] that the balance between the rate of decomposition and the rate of oxidation of carbon define the overall stability of the catalyst.

The slight change in the intensities of CO_2 peak of the catalysts (Fig. 7) is most likely due to the difference in the number of carbon atoms available on the catalyst surface. The lowest intensity of the peak for ceria-supported Pt catalyst is due to the low carbon deposition caused by the higher oxygen storage capacity of CeO_2 [8,49]. It can be concluded that ceria has the ability to accelerate the oxygen exchange capacity; the high rate of oxygen transfer helps to keep the metal surface free of carbon with time on stream. This leads to maintain the high activity of the catalysts that can be explained by the bifunctional mechanism for reforming proposed by many authors [1,49,54], in which the role of the support is very important. CO_2 is activated on the support, whereas methane is activated on the metal. The two activated species may react with each other on the Pt-support boundary.

5. Conclusions

From this work, the following conclusions can be drawn: (i) Pt/CeO_2–ZrO_2 catalysts with high surface area and mesoporous nanocrystalline structure of zirconia carrier are obtained. The small amount of CeO_2 up to 6 wt% has stabilization effect on the textural properties of modified ZrO_2 with CeO_2; (ii) fully reduced and well-dispersed Pt on the surface of Pt/CeO_2–ZrO_2 catalysts leads to an acceleration of CH_4 decomposition; (iii) addition of CeO_2 to Pt/ZrO_2 catalyst prevents the deactivation of the catalyst by acceleration of gasification of coke deposition on Pt particles. This is related to the increase of the oxygen mobility on the surface of the support due a close contact between Pt and ceria.

Acknowledgments

The authors gratefully acknowledge Dr. M.A. Peña (ICP-CSIC) for the DTA/TGA measurements. Financial support by CSIC (Spain), CAM (Project CCG07-CSIC/ENE-1884) and NFS-Bulgaria (project X-1515/05) is acknowledged. S.D. thanks the Ministry of Education and Culture (Spain) for a sabbatical year grant No. SAB2005/0035.

References

[1] M.C.J. Bradford, M.A. Vannice, Catal. Rev. Sci. Eng. 41 (1999) 1.
[2] J.R. Rostrup-Nielsen, Stud. Surf. Sci. Catal. 81 (1994) 25.
[3] R.M. Navarro, M.A. Peña, J.L.G. Fierro, Chem. Rev. 197 (2007) 3952.
[4] I. Alstrup, M.T. Tavares, J. Catal. 135 (1992) 147.
[5] V.C.H. Kroll, H.M. Swaan, C. Mirodatos, J. Catal. 161 (1996) 409.
[6] M.E.S. Hegarty, A.M. O'Connor, J.R.H. Ross, Catal. Today 42 (1998) 22.
[7] S.M. Gheno, S. Damyanova, B.A. Riguetto, C.M.P. Marques, C.A.P. Leite, J.M.C. Bueno, J. Mol. Catal. A: Gen. 198 (2003) 263.
[8] S. Damyanova, J.M.C. Bueno, Appl. Catal. A: Gen. 253 (2003) 135.
[9] A.C.S.F. Santos, S. Damyanova, G.N.R. Teixeira, L.V. Mattos, F.B. Noronha, F.B. Passos, J.M.C. Bueno, Appl. Catal. A: Gen. 290 (2005) 197.
[10] L.S.F. Feio, C.E. Hori, S. Damyanova, F.B. Noronha, W.H. Cassinelli, C.M.P. Marques, J.M.C. Bueno, Appl. Catal. A: Gen. 316 (2007) 107.
[11] E. Aneggi, M. Boaro, C. De Leitenburg, G. Dolcetti, A. Trovarelli, J. Alloys Compd. 408–412 (2006 1096).
[12] F.B. Norohna, E.C. Fendley, R.R. Soares, W.E. Alvarez, D.E. Resasco, Chem. Eng. J. 82 (2001) 21.
[13] R. Wang, H. Xu, X. Liu, Q. Ge, W. Li, Appl. Catal. A: Gen. 305 (2006) 204.
[14] L.F. Liotta, G. Di Carlo, G. Pantaleo, G. Deganello, Appl. Catal. B: Environ. 70 (2007) 314.
[15] Y. Denkwitz, A. Karpenko, V. Pizak, R. Leppelt, B. Schumacher, R.J. Behm, J. Catal. 246 (2007) 74.
[16] A. Pintar, J. Batista, S. Hocever, J. Colloid Interface Sci. 307 (2007) 145.
[17] M. Rezaei, S.M. Alavi, S. Sahebdelfar, Z.E. Yan, Mater. Lett. 61 (2007) 2628.
[18] P. Bera, K.C. Ratil, V. Jayaram, G.N. Sublanna, M.S. Hegde, J. Catal. 196 (2000) 293.
[19] S. Damyanova, B. Pawelec, K. Arishtirova, M.V. Martinez Huerta, J.L.G. Fierro, Appl. Catal. A: Gen. 337 (2008) 86.
[20] H.P. Klug, L.E. Alexander, X-ray Diffraction Procedures for Polycrystalline and Amorphous Materials, 2nd ed., Wiley-Interscience, New York, 1974.
[21] D.A. Shirley, Phys. Rev. B5 (1972) 4709.
[22] P.M.A. Sherwood, in: D. Briggs, M.P. Seah (Eds.), Practical Surface Analysis, Wiley, New York, 1990, p. 181.
[23] G. Leofanti, M. Padovan, G. Tozzola, B. Venturelli, Catal. Today 41 (1998) 207.
[24] V.R. Mastelaro, V. Briois, D.P.F. de Soza, C.L. Silva, J. Eur. Ceram. Soc. 23 (2003) 273.
[25] S. Eriksson, S. Rojas, M. Boutonnet, J.L.G. Fierro, Appl. Catal. A: Gen. 326 (2007) 8–16.
[26] P.D.L. Mercera, J.G. van Ommen, E.B.M. Doesburg, A.J. Burggraaf, J.R.H. Ross, Appl. Catal. 57 (1990) 127.
[27] S. Damyanova, C.A. Perez, M. Schmal, J.M.C. Bueno, Appl. Catal. A: Gen. 184 (2002) 271.
[28] E.F. Lopez, V.S. Escribiano, M. Panizza, M.M. Carnasciali, G. Busca, J. Mater. Chem. 11 (2001) 1891.
[29] S. Wang, W. Wang, J. Zuo, Y. Qian, Mater. Chem. Phys. 68 (2001) 246.
[30] M. Yashima, M.K. Morimoto, N. Ishizawa, M. Yoshimura, J. Am. Ceram. Soc. 76 (1993) 1745.
[31] J.E. Spanier, R.D. Robinson, F. Zhang, S.W. Chan, I.P. Herman, Phys. Rev. B 64 (2001) 245407.
[32] W. Yang, Y. Ma, J. Tang, X. Yang, Colloids Interface A: Phys. Eng. Aspects 302 (2007) 628.
[33] Z. Yi, W. Wei, S. Lee, G. Jianhna, Catal. Commun. 8 (2007) 906.
[34] B.A. Riquetto, S. Damyanova, G. Gouliev, C.M. Marques, L. Petrov, J.M.C. Bueno, J. Phys. Chem. B 108 (2004) 5349.
[35] S. Tsunekawa, K. Asami, S. Ito, M. Yashima, T. Sugimoto, Appl. Surf. Sci. 252 (2005) 1651.
[36] S. Damyanova, P. Grange, B. Delmon, J. Catal. 168 (1997) 421.
[37] P. Burroughs, A. Hamnett, A.F. Orchard, G. Thornton, J. Chem. Soc., Dalton Trans. 17 (1976) 1686.
[38] J.M. Pigos, C.J. Brooks, G. Jacobs, B.H. Davis, Appl. Catal. A: Gen. 319 (2007) 47.
[39] P. Fornasiero, R. Di Monte, G.R. Rao, J. Kašpar, S. Meriani, A. Trovarelli, M. Graziani, J. Catal. 151 (1995) 168.
[40] M. Daturi, C. Binet, J.C. Lavalley, A. Galtayries, R. Sporken, Phys. Chem. Chem. Phys. 1 (1999) 5717.
[41] A. Galtayries, R. Sporken, J. Riga, G. Blanchard, R. Caudano, J. Electron Spectrosc. Relat. Phenom. 88–91 (1998) 951.
[42] C.D. Wagner, L.E. Davis, M.V. Zeller, J.A. Taylor, R.H. Raymond, L.H. Gale, Surf. Interface Anal. 3 (1981) 211.
[43] G. Jacobs, P.M. Patterson, L. Williams, D. Sparks, B.H. Davis, Catal. Lett. 96 (2004) 97105.
[44] J.E. Fallah, S. Boujana, H. Dexpert, A. Kiennemann, J. Majerus, O. Touret, F. Villin, F.L. Normand, J. Phys. Chem. 98 (1994) 5522.
[45] G. Jacobs, U.M. Graham, E. Chenu, P.M. Paterson, A. Dozier, B.H. Davis, J. Catal. 229 (2005) 499.
[46] H. Lieske, G. Lictz, H. Spindler, J. Volter, J. Catal. 81 (1983) 8.
[47] J.Z. Shyu, K. Otto, J. Catal. 115 (1989) 16.
[48] C. de Lietenburg, A. Trovarelli, J. Kaspar, J. Catal. 166 (1997) 98.
[49] F.B. Noronha, A. Shamsi, C. Taylor, E.C. Fendley, S. Stagg-Williams, D.E. Resasco, Catal. Lett. 90 (2003) 13.
[50] S.M. Stagg, D.E. Desasco, Stud. Surf. Sci. Catal. 119 (1998) 813.
[51] S. Bernal, M.A. Cauqui, G.A. Cifredo, J.M. Gatica, C. Larese, J.A. Perez Omil, Catal. Today 29 (1996) 77.
[52] J. Fan, X. Wu, R. Ran, D. Weng, Appl. Surf. Sci. 245 (2005) 162.
[53] J.H. Bitter, K. Seshan, J.A. Lercher, J. Catal. 171 (1997) 279.
[54] K. Nagaoka, K. Seshan, K. Aika, J.A. Lercher, J. Catal. 197 (2001) 34.
[55] A.M. O'Conor, Y. Schurman, J.R.H. Ross, C. Mirodatos, Catal. Today 115 (2006) 191.
[56] A.M. Efstathiou, A. Kladi, V.A. Tsipouriari, X.E. Verykios, J. Catal. 158 (1996) 64.
[57] D.G. Rethwich, J.A. Dumesic, Appl. Catal. 21 (1986) 97.